Asian Review of Mechanical Engineering
ISSN: 2249-6289 (P) Vol.11 No.1, 2022, pp.40-52

DOI: https://doi.org/10.51983/arme-2022.11.1.3346

Sensor and Process Noises Reduction using a Luenberger State Estimator with a Stability Augmentation System for a Hypersonic Transport Aircraft

Zairil A. Zaludin
Department of Aerospace, Faculty of Engineering, Universiti Putra Malaysia, Selangor, Malaysia
E-mail: zairil_azhar@upm.edu.my
(Received 12 April 2022; Accepted 19 May 2022; Available online 25 May 2022)

***Abstract* - This paper firstly, presents an autopilot strategy for a Hypersonic Transport Aircraft (HST) using a Stability Augmentation System (SAS) with a Luenberger estimator. The SAS is designed using Linear Quadratic Regulator (LQR) theory which, for HST, benefits the guaranteed robust dynamic stability provided three theoretical requirements are met. The Luenberger estimator is incorporated into the autopilot design to estimate the state variables of the aircraft for the SAS. In the dynamic response simulation, sensor and process noises are inserted into the mathematical model. However, to date, knowledge of the sensor and process noises at the speeds and heights where the aircraft will be flying is limited. The simulation shows that the Luenberger estimator significantly filters the noise. This is an advantage for the HST as prior knowledge of the noises is not necessary when designing the Luenberger estimator.**
***Keywords:* Hypersonic Aircraft, LQR Theory, Luenberger State Estimator, Sensor Noise Reduction, Process Noise Reduction**

NOMENCLATURE

As scientific texts use different notations applied in this paper are mentioned below.

h	Aircraft altitude (ft)
θ	Pitch attitude (rad)
α	Angle of attack (rad)
m	Vehicle mass per unit width (slug/ft)
m	Generalised elastic mass per unit width (slug/ft)
U_o	Flight Speed (ft/s)
w	Vertical velocity (ft/s)
q	Pitch rate (rad/s)
X,Y,Z	Force components of body axis (lb)
I_{yy}	Pitching moment of inertia (slugs.ft^2)
M	Pitching moment (lb.ft)
M_∞	Mach number at freestream condition
a_∞	Speed of sound (ft/s)
ω_1	Natural frequency of first in vacuo vibration mode (rad/s)
ζ_1	Damping ratio of first in vacuo vibration mode
$\boldsymbol{x}$	State vector
A	State Coefficient Matrix
B	Control Coefficient Matrix
$\boldsymbol{u}$	Control vector
Δ	Perturbation of aircraft state variable from trimmed condition
u	Forward speed (ft/s)
η	Generalised elastic coordinate (rad)
δ_F	Flap deflection (rad)
A_D	Propulsion diffuser area ratio
T_o	Total temperature across combustor (^{o}R)
y	Output vector
C	Output Coefficient Matrix
K	State feedback gain matrix
P	Solution to the algebraic Riccati equation
X_x	Partial derivative of the total force along X axis with respect to x
g	Acceleration due to gravity (ft/s^2)
c_1	Pressure coefficient
$\Delta\tau_1$	Vehicle nose angle from side view (rad)
Z_x	Partial derivative of the total force along Z axis with respect to x
λ	Eigenvalues of aircraft without feedback control system
I	Identity Matrix
$\boldsymbol{x_E}$	Estimated state vector (from the Luenberger estimator)
$\widehat{\mathrm{F}}$	Coefficient State Matrix (from the Luenberger estimator)
$\widehat{\mathrm{G}}$	Coefficient Control Matrix (from the Luenberger estimator)
$\mathrm{K_E}$	Estimator gain matrix
$\boldsymbol{y_E}$	Estimated output vector
$\boldsymbol{e}$	Difference between the estimated and the actual state vector
$\tilde{\boldsymbol{v}}$	State Estimator Feedback Control Law
$\mathrm{G_o}$	Control weighting matrix (to find a Luenberger Estimator matrix)
Q	State weighting matrix (to find a state feedback gain matrix)
G	Control weighting matrix (to find a state feedback gain matrix)
rms	Root mean square value

I. INTRODUCTION

Hypersonic fight vehicle (HFV) has a flight speed exceeding 5 times the speed of sound. This vehicle has dual capability to fly as a spacecraft and an aircraft and has significant military value and potential economic value [1]. The system states of HFV are usually difficult to be accurately measured due to sensor noises and complex flight environment, which makes the controller design extremely difficult. In [2], the tracking control problem of hypersonic flight vehicle (HFV) with measurement noises and system uncertainties were investigated. To deal with such a problem, a linear quadratic Gaussian (LQG) optimal control algorithm and a robust back-stepping control strategy are proposed using Kalman filter. In [3], the augmented fixed-time observers and adaptive super-twisting controller are combined to ensure the superior tracking performances of HFV under the effects of uncertainties, disturbances, and measurement noises.

In this paper, the method of designing, by means of the optimal Linear Quadratic Regulator (LQR) theory, an effective Stability Augmentation System (S.A.S) to stabilise the longitudinal dynamics of an aircraft flying at a hypersonic speed is first described. LQR theory has considerable practical advantages for use in Automatic Flight Control System (AFCS) design, particularly for the hypersonic transport (HST) aircraft, since it guarantees robust closed-loop dynamic stability as long as three theoretical requirements are met [4,5]. However, the optimal LQR control law requires that all the state variables of the aircraft be measurable. This is impractical but with the use of a Luenberger state estimator, LQR theory is practical although it involves a slight loss in optimality [4,5,6,7].

A dynamic simulation shows that the longitudinal dynamics of the HST aircraft, with the controller and the estimator operating together, were found to remain stable. It was found also that the response of the estimated state vector generated by the Luenberger estimator quickly reached that of the hypersonic aircraft even when the aircraft was subjected to disturbances or to command inputs. The paper also shows that the Luenberger state estimator is able to reduce the output noise present in the HST dynamics even when there are aircraft sensor noise and process noise present. This is advantageous to an HST aircraft flying at a range of high Mach numbers and heights because knowledge of the sensor and process noises at these speeds and heights is limited [8].

In this paper, the mathematical model of the aircraft is firstly introduced. Then, the state of the aircraft static and dynamic stability is briefly analysed. Using optimal Linear Quadratic Regulator theory, a Stability Augmentation System is designed and a Luenberger estimator is incorporated into the autopilot system. Finally, the sensor and process noise reduction capability of the SAS with Luenberger estimator is demonstrated.

II. THE MATHEMATICAL MODEL OF THE HYPERSONIC AIRCRAFT LONGITUDINAL MOTION

The mathematical model of the hypersonic aircraft presented in this paper is based on the mathematical model of the X-30 Reusable Launch Vehicle (RLV) published by Chavez and Schmitt [9]. However, the published mathematical model had to be developed further to suit the needs of the research work published in this paper. Details of the modifications are presented in [10]. The X-30 configuration [9], is shown in Figure 1.

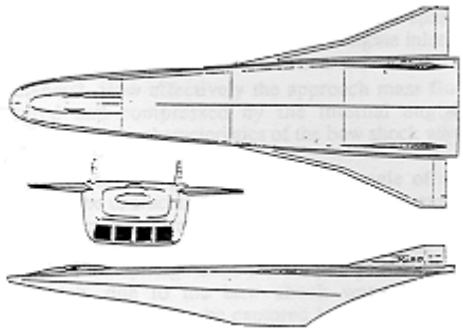

Fig. 1 X-30

The longitudinal equations of motion to be considered here are

$$\dot{h} = U_o \sin(\theta - \alpha) \tag{1}$$

$$m(\dot{u} + wq) = X - mg\sin(\theta) \tag{2}$$

$$m(\dot{w} - uq) = Z + mg\cos(\theta) \tag{3}$$

$$I_{yy}\dot{q} = M \tag{4}$$

Equations (1 – 4), linearised with respect to an equilibrium flight condition, yield the linearised perturbation equations:

$$\Delta\dot{h} = -U_o\Delta\alpha + U_o\Delta\theta \tag{5}$$

$$\Delta\dot{u} = -g\Delta\theta + \frac{\Delta X}{m} \tag{6}$$

$$\Delta\dot{\alpha} = \frac{\Delta\dot{w}}{U_o} = \Delta q + \frac{\Delta Z}{U_o m} \tag{7}$$

$$\Delta\dot{\theta} = \Delta q \tag{8}$$

$$\Delta\dot{q} = \frac{\Delta M}{I_{yy}} \tag{9}$$

where $U_o = M_\infty a_\infty$, g is the acceleration due to gravity and the delta quantities are the perturbations from the equilibrium flight condition. With undamped natural frequency ω_1 and damping ratio ζ_1 the perturbed equation of motion describing the elastic degree of freedom is governed by

$$\Delta\ddot{\eta} = -\omega_1^2\Delta\eta - 2\zeta_1\omega_1\Delta\dot{\eta} + \frac{\Delta Q}{\mathrm{m}} \tag{10}$$

Based on the method in [9], and the modifications reported in [7], the mathematical model of the HST aircraft used in this work which forms the basis of this paper was represented by a linear, time-invariant, state equation

$$\dot{\boldsymbol{x}} = \mathrm{A}\boldsymbol{x} + \mathrm{B}\boldsymbol{u} \qquad (11)$$

$\boldsymbol{x} \in \mathrm{R}^n$ represents the state vector and $\boldsymbol{u} \in \mathrm{R}^m$ represents the control vector. A is the state coefficient matrix and B is the driving matrix, of order (n×n) and (n×m) respectively.

If, for example, the aircraft dynamics has 7 state variables and 3 control variables, then n = 7 and m = 3. The state and the control variables are defined in Eqn (12) and (13). viz.

$$\boldsymbol{x} = \begin{bmatrix} \Delta u\,(\mathrm{ft/s}) \\ \Delta \alpha\,(\mathrm{rad}) \\ \Delta q\,(\mathrm{rad/s}) \\ \Delta \theta\,(\mathrm{rad}) \\ \Delta h\,(\mathrm{ft}) \\ \Delta \eta\,(\mathrm{rad}) \\ \Delta \dot{\eta}\,(\mathrm{rad/s}) \end{bmatrix} \qquad (12)$$

$$\boldsymbol{u} = \begin{bmatrix} \Delta \delta_F\,(\mathrm{rad}) \\ \Delta A_D \\ \Delta T_o\,(^{\circ}\mathrm{R}) \end{bmatrix} \qquad (13)$$

The variables are all perturbations from an equilibrium flight condition. The output equation is represented by the Eqn (14) below

$$\mathrm{y} = \mathrm{Cx} \qquad (14)$$

where $\boldsymbol{y}$ is the output vector and C is the output matrix.

The complete procedure for obtaining the coefficient matrices, A and B, at different flight conditions for the HST aircraft is presented in [9] and [10]. Shown below are the formula obtained to develop the matrices A and B at various flight conditions.

$$A = \begin{bmatrix} \frac{X_{M_\infty}}{a_\infty m} & \frac{X_\alpha}{m} & \frac{X_q}{m} & -g & \frac{c_1 X_{M_\infty}}{m} & \frac{X_\eta}{m\Delta\tau_1} & \frac{X_{\dot\eta}}{m\Delta\tau_1} \\ \frac{Z_{M_\infty}}{a_\infty m U_o} & \frac{Z_\alpha}{mU_o} & \left[1+\frac{Z_q}{mU_o}\right] & 0 & \frac{c_1 Z_{M_\infty}}{mU_o} & \frac{Z_\eta}{mU_o\Delta\tau_1} & \frac{Z_{\dot\eta}}{mU_o\Delta\tau_1} \\ \frac{M_{M_\infty}}{a_\infty I_{yy}} & \frac{M_\alpha}{I_{yy}} & \left[1+\frac{M_q}{I_{yy}}\right] & 0 & \frac{c_1 M_{M_\infty}}{I_{yy}} & \frac{M_\eta}{I_{yy}\Delta\tau_1} & \frac{M_{\dot\eta}}{I_{yy}\Delta\tau_1} \\ 0 & 0 & 0 & 0 & 0 & 0 & 0 \\ 0 & -U_o & 0 & U_o & 0 & 0 & 0 \\ 0 & 0 & 0 & 0 & 0 & 0 & 0 \\ \frac{Q_{M_\infty}\Delta\tau_1}{a_\infty \mathrm{m}} & \frac{Q_\alpha\Delta\tau_1}{\mathrm{m}} & \frac{Q_q}{\mathrm{m}} & 0 & \frac{c_1 Q_{M_\infty}\Delta\tau_1}{\mathrm{m}} & \frac{Q_\eta}{\mathrm{m}} - \omega_1^2 & \frac{Q_{\dot\eta}}{\mathrm{m}} - 2\zeta_1\omega_1 \end{bmatrix} \qquad (15)$$

$$B = \begin{bmatrix} \frac{X_{\delta_F}}{m} & \frac{X_{A_D}}{m} & \frac{X_{T_o}}{m} \\ \frac{Z_{\delta_F}}{mU_o} & \frac{Z_{A_D}}{mU_o} & \frac{Z_{T_o}}{mU_o} \\ \frac{M_{\delta_F}}{I_{yy}} & \frac{M_{A_D}}{I_{yy}} & \frac{M_{T_o}}{I_{yy}} \\ 0 & 0 & 0 \\ 0 & 0 & 0 \\ 0 & 0 & 0 \\ \frac{Q_{\delta_F}\Delta\tau_1}{\mathrm{m}} & \frac{Q_{A_D}\Delta\tau_1}{\mathrm{m}} & \frac{Q_{T_o}\Delta\tau_1}{\mathrm{m}} \end{bmatrix} \qquad (16)$$

To obtain the findings presented in this paper, the aircraft was simulated to be flying at Mach 8.0 and at an altitude of 85,000ft. The stability and control derivatives obtained from [9,10] show the individual contributions of aerodynamics, engine thrust and exhaust gas. Then, these individual contributions are added up to obtain the total values. The results are tabulated below.

TABLE I STABILITY AND CONTROL DERIVATIVES FOR AIRCRAFT FLYING AT MACH 8.0 AND AT A HEIGHT OF 85000FT

Stability Derivatives					
Symbol	**Aerodynamics Contribution**	**Engine Thrust Contributions**	**Exhaust Gas Contributions**	**Total**	**Units**
X_{M_∞}	-3.5860×10^{3}	1.3755×10^{3}	1.5725×10^{2}	-2.0533×10^{3}	lb/ft
X_α	-7.6496×10^{4}	5.4504×10^{4}	4.4770×10^{3}	-1.7515×10^{4}	(lb/ft)/rad
X_q	2.1784×10^{2}	-4.0782	-3.3498×10^{-1}	2.1343×10^{2}	(lb/ft)/(rad/s)
X_η	-1.0084×10^{3}	9.5128×10^{2}	2.1951×10^{2}	1.6244×10^{2}	(lb/ft)/rad
$X_{\dot\eta}$	3.7529	0.0	0.0	3.7529	(lb/ft)/(rad/s)
Z_{M_∞}	-8.4842×10^{3}	0.0	-4.3193×10^{2}	-8.9161×10^{3}	lb/ft
Z_α	-2.1813×10^{5}	0.0	-1.2298×10^{4}	-2.3042×10^{5}	(lb/ft)/rad
Z_q	8.7362×10^{2}	0.0	9.2013×10^{-1}	8.7454×10^{2}	(lb/ft)/(rad/s)
Z_η	-2.5446×10^{3}	0.0	-1.6317×10^{2}	-2.7078×10^{3}	(lb/ft)/rad
$Z_{\dot\eta}$	1.5051×10^{1}	0.0	0.0	1.5051×10^{1}	(lb/ft)/(rad/s)

M_{M_∞}	-2.3513×10^{4}	1.5062×10^{4}	-8.3443×10^{2}	-9.2858×10^{3}	lb
M_{α}	3.7699×10^{6}	5.9682×10^{5}	-2.3757×10^{4}	4.3430×10^{6}	lb/rad
M_{q}	-5.7842×10^{4}	-4.4656×10^{1}	1.7776	-5.7885×10^{4}	lb/(rad/s)
M_{η}	1.1589×10^{5}	1.0417×10^{4}	1.0834×10^{3}	1.2739×10^{5}	lb/rad
$M_{\dot{\eta}}$	-9.2234×10^{2}	0.0	0.0	-9.2234×10^{2}	lb/(rad/s)
Q_{M_∞}	3.3070×10^{3}	0.0	5.1928×10^{1}	3.3589×10^{3}	lb
Q_{α}	1.2446×10^{5}	0.0	1.4784×10^{3}	1.2594×10^{5}	lb/rad
Q_{q}	-9.5815×10^{2}	0.0	-1.1062×10^{-1}	-9.5826×10^{2}	lb/(rad/s)
Q_{η}	2.1723×10^{3}	0.0	2.5804×10^{1}	2.1981×10^{3}	lb/rad
$Q_{\dot{\eta}}$	-1.6560×10^{1}	0.0	0.0	-1.6560×10^{1}	lb/(rad/s)

Control Derivatives					
Symbol	**Aerodynamics**	**Engine Thrust**	**Exhaust Gas**	**Total**	**Units**
X_{δ_F}	-5.6795×10^{4}	0.0	0.0	-5.6795×10^{4}	(lb/ft)/rad
X_{A_D}	0.0	-7.8975×10^{4}	-6.8185×10^{3}	-8.5793×10^{4}	lb/ft
X_{T_o}	0.0	6.4254	2.3888×10^{-1}	6.6643	(lb/ft)/deg R
Z_{δ_F}	-5.6954×10^{4}	0.0	0.0	-5.6954×10^{4}	(lb/ft)/rad
Z_{A_D}	0.0	0.0	1.8729×10^{4}	1.8729×10^{4}	lb/ft
Z_{T_o}	0.0	0.0	-6.5617×10^{-1}	-6.5617×10^{-1}	(lb/ft)/deg R
M_{δ_F}	-2.3511×10^{6}	0.0	0.0	-2.3511×10^{6}	lb/rad
M_{A_D}	0.0	-8.6477×10^{5}	3.6182×10^{4}	-8.2859×10^{5}	lb
M_{T_o}	0.0	7.0358×10^{1}	-1.2676	6.9090×10^{1}	lb/deg R
Q_{δ_F}	0.0	0.0	0.0	0.0	lb/rad
Q_{A_D}	0.0	0.0	-2.2517×10^{3}	-2.2517×10^{3}	lb
Q_{T_o}	0.0	0.0	7.8887×10^{-2}	7.8887×10^{-2}	lb/deg R

At that flight condition, using Eqn (15) and (16), the corresponding matrices A, and B could be shown to be:

$$A = \begin{bmatrix} -4.1857\times10^{-3} & -35.03 & 4.2686\times10^{-1} & -32.2 & 7.9938\times10^{-4} & 18.614 & 4.3006\times10^{-1} \\ -2.3158\times10^{-6} & -5.8716\times10^{-2} & 1.0002 & 0 & 4.4227\times10^{-7} & -3.9534\times10^{-2} & 2.1974\times10^{-4} \\ -9.4647\times10^{-6} & 4.3430 & -5.7885\times10^{-2} & 0 & 1.8076\times10^{-6} & 7.2990 & -5.2846\times10^{-2} \\ 0 & 0 & 1 & 0 & 0 & 0 & 0 \\ 0 & -7.8487\times10^{3} & 0 & 7.8487\times10^{3} & 0 & 0 & 0 \\ 0 & 0 & 0 & 0 & 0 & 0 & 1 \\ 1.4938\ 10^{-3} & 54.95 & -4.1812\times10^{-1} & 0 & -2.8529\times10^{-4} & -2.6905\times10^{2} & -1.1340 \end{bmatrix} \quad (17)$$

$$B = \begin{bmatrix} -1.4376\times10^{2} & -1.8197\times10^{2} & 1.4648\times10^{-2} \\ -1.6327\times10^{-2} & 4.3490\times10^{-3} & -1.5433\times10^{-7} \\ -2.9757 & -8.9451\times10^{-1} & 7.6588\times10^{-5} \\ 0 & 0 & 0 \\ 0 & 0 & 0 \\ 0 & 0 & 0 \\ 0 & -9.1702\times10^{-1} & 3.2542\ 10^{-5} \end{bmatrix} \quad (18)$$

III. THE RESPONSE OF THE AIRCRAFT DYNAMICS TO COMMANDED INPUT

It is common practice to check the nature of stability of an aircraft before any AFCS is designed. The nature of the aircraft static stability can be measured from a knowledge of the aircraft change in pitching moment with respect to the change in angle of attack, M_α [7].

M_α, is found to be 4.3430×10^6 lb/rad. It can be seen here that the aircraft is *statically unstable* since the change in pitching moment in one direction will also result in a change in the angle of attack in the same direction. Hence, the aircraft has no natural tendency to return to its equilibrium state when it is subjected to gust or other similar disturbance. The other point of interest to note here is that the level of static instability of the aircraft is exceptionally high, of the order 10^6. This is higher than usual when compared to that of any other aircraft known to be flying today,

The dynamic stability of the aircraft can be analysed from the eigenvalues of the coefficient matrix, A. These eigenvalues can be calculated by solving Eqn (19) shown below.

$$\det\left[\lambda \mathrm{I} - \mathrm{A}\right] = 0 \qquad (19)$$

where I is an identity matrix and λ is the eigenvalue set.

By solving the characteristic equation of the matrix [λI – A], the eigenvalues of the HST were found and shown below.

$\lambda_1 = 2.33$
$\lambda_2 = -2.49$
$\lambda_3 = 0$
$\lambda_{4,5} = -1.89\times10^{-3} \pm j5.78\times10^{-2}$
$\lambda_{6,7} = -0.55 \pm j16.4$

λ_1 is a positive real number which implies that the aircraft is dynamically unstable [7]. To confirm this, the response of the aircraft to a 5-degree step input change in angle of deflection to the flaps is simulated using Matlab® and Simulink® software. The block diagram of the aircraft dynamics used for the Simulink software can be seen below.

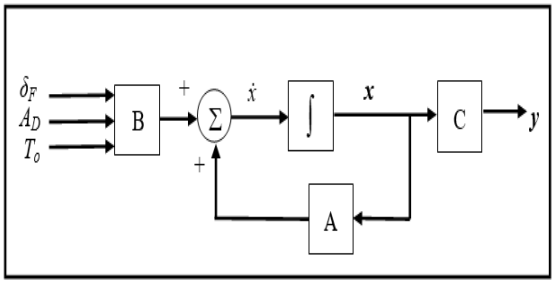

Fig. 2 The Block Diagram of the Aircraft dynamics

Figure 3 shows the responses of the aircraft state variables. It can be seen here that the aircraft dynamics are unstable as the responses do not approach any steady state value but instead increase indefinitely.

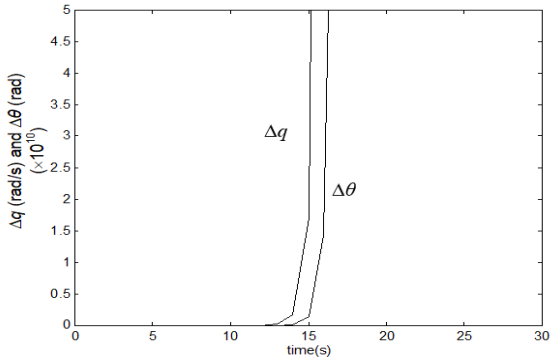

Fig. 3 Dynamic responses of Hyperion pitch attitude, θ, and pitch rate, q, to a 5-degree step input change in flap angle

IV. STABILIZATION OF THE LONGITUDINAL MOTION OF HYPERION

The HST dynamics have been shown to suffer from instability problems. The method of designing an effective Stability Augmentation System (S.A.S) for the HST to stabilise the aircraft dynamics based on LQR theory is described in this section. Without any S.A.S, the HST showed highly unstable dynamic response. How LQR theory was used to obtain an optimal feedback control law which stabilised the aircraft dynamics is described next.

The LQR theory can be stated as follows. Find a feedback gain K so that the performance index

$$J = \frac{1}{2}\int_0^\infty \left[x'Qx + u'Gu\right]dt \qquad (20)$$

is minimised. The solution to this problem is well known [4,5,6]. The feedback gain K that solves the LQR problem is given by:

$$\mathrm{K} = -\mathrm{G}^{-1}\mathrm{B}'\mathrm{P} \qquad (21)$$

where P is the solution to the algebraic matrix Riccati equation:

$$\mathrm{A}'\mathrm{P} + \mathrm{PA} - \mathrm{PBG}^{-1}\mathrm{B}'\mathrm{P} + \mathrm{Q} = 0 \qquad (22)$$

To guarantee the existence of a unique solution, G must be positive definite ($G > 0$). A sufficient condition for the existence of a solution P for the Riccati equation is that Q must be positive semidefinite ($Q \geq 0$). How the controller is incorporated into the aircraft dynamics is shown next. The block diagram of the aircraft dynamics is shown below.

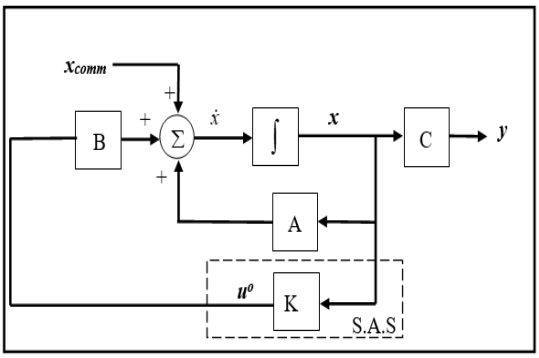

Fig. 4 Aircraft dynamics with a Stability Augmentation System (S.A.S)

x_{comm} is the command input for the controlled aircraft dynamics, and is a vector of dimension, n. Note that the command input is inserted into the aircraft dynamics as a commanded change in the state of the aircraft.

For the HST dynamics, the matrices, Q and G, which were chosen for the performance index given in Eqn (20) are presented below.

$$Q = \text{diag}\left[1.0 \quad 5.0 \quad 10.0 \quad 0.1 \quad 1\times10^{-5} \quad 0.0 \quad 0.0\right] \qquad (23)$$

$$G = \text{diag}\left[1.0 \quad 1.0 \quad 1.0\right] \qquad (24)$$

The choice of the elements for the matrix, Q, was made to stabilise the short period mode. High penalties were placed on any changes in the angle of attack, $\Delta\alpha$, (e.g., in Eqn (22); Q(2,2) = 5.0) and the pitch rate, Δq (Q(3,3) = 10.0). This choice of weighting elements was made to penalise any persistent motions involving these state variables. At this time, no penalty was applied to any changes in structural bending, $\Delta\eta$ and $\Delta\dot{\eta}$ because the contributions of these variables towards the aircraft instability were uncertain. The other diagonal elements of the matrix, Q, were chosen completely arbitrarily. The three controls, δ_F, A_D and T_o were penalised equally as can be seen from the matrix, G, of Eqn (24). Note that the matrix, Q, was positive semidefinite; the matrix, G was positive definite.

A solution to the associated Riccati equation was found by using a routine in the Matlab Control System Toolbox. The resulting matrix was

$$P = \begin{bmatrix} 0.005 & 0.593 & -0.043 & -0.708 & -3.8\times10^{-5} & -0.008 & -0.001 \\ 0.593 & 3555.1 & -69.1 & -3852.4 & -0.244 & -13.98 & -2.149 \\ -0.043 & -69.1 & 4.61 & 81.58 & 0.005 & 0.891 & 0.115 \\ -0.708 & -3852.4 & 81.58 & 4200.3 & 0.263 & 16.09 & 2.49 \\ -3.8\times10^{-5} & -0.244 & 0.005 & 0.263 & 2.6\times10^{-5} & 0.0009 & 0.0001 \\ -0.008 & -13.98 & 0.891 & 16.09 & 0.0009 & 0.91 & 0.02 \\ -0.001 & -2.149 & 0.115 & 2.49 & 0.0001 & 0.02 & 0.0059 \end{bmatrix} \qquad (25)$$

This solution, P, to the algebraic Riccati equation is both symmetrical and positive definite. Using Eqn (21), the optimal feedback gain matrix can then be calculated. It is shown below as Eqn (26).

$$K' = \begin{bmatrix} -0.505 & -0.86 & 6.7\times10^{-5} \\ 43.57 & -25.33 & 0.002 \\ -4.99 & 3.05 & -0.0002 \\ -55.48 & 33.03 & -0.003 \\ -0.003 & 0.002 & -1.6\times10^{-7} \\ -0.996 & 0.524 & -4.0\times10^{-5} \\ -0.119 & 0.07 & -5.7\times10^{-6} \end{bmatrix} \qquad (26)$$

The dynamic stability of an aircraft with closed-loop control can be determined by solving Eqn (27). A controlled aircraft is dynamically stable if all the real eigenvalues of the closed-loop eigenvalues or the real parts of these eigenvalues are negative [4,5,6,7].

$$\det\left[\zeta I - (A - B\times K)\right] = 0 \qquad (27)$$

From Eqn (27), After stabilisation the eigenvalues of the HST were found using Eqn (27). All the closed-loop eigenvalues of the optimally controlled HST can be deduced to possess negative real parts which indicates that the controlled aircraft will be dynamically stable. These are shown in Table II.

TABLE II HYPERION'S CLOSED-LOOP EIGENVALUES FLYING AT MACH 8.0 AND AT A HEIGHT OF 85000FT

Closed - Loop Eigenvalues	Natural Frequencies	Damping Ratios	Motion Represented
$\zeta_{1,2}$ = -0.52 ± j0.6	0.79 rad/s	0.66	Phugoid
$\zeta_{3,4}$ = -0.55 ± j16.428	16.4 rad/s	0.03	Structural Bending
ζ_5 = -5.765	-	-	Short Period
ζ_6 = -205.87	-	-	Short Period
ζ_7 = -1.3288	-	-	Height

The responses of the stabilised aircraft to an initial disturbance in height are shown in Figure 5. These responses indicate that the controlled aircraft is dynamically stable whenever it is subjected to disturbances.

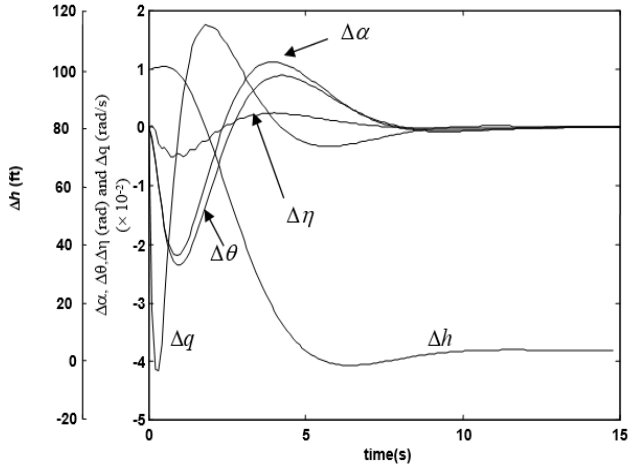

Fig. 5 The closed-loop dynamic responses when Hyperion was subjected to an initial disturbance in height of 100ft

In Figure 5, the oscillation of the phugoid motion is evident on every response. The period of oscillation is approximately 8 seconds. The oscillation of the structural bending motion can be seen on the $\Delta\eta$ initial disturbance response curve. This comes about as a consequence of not applying enough penalties to the change in the structural bending state variable and its rate of change.

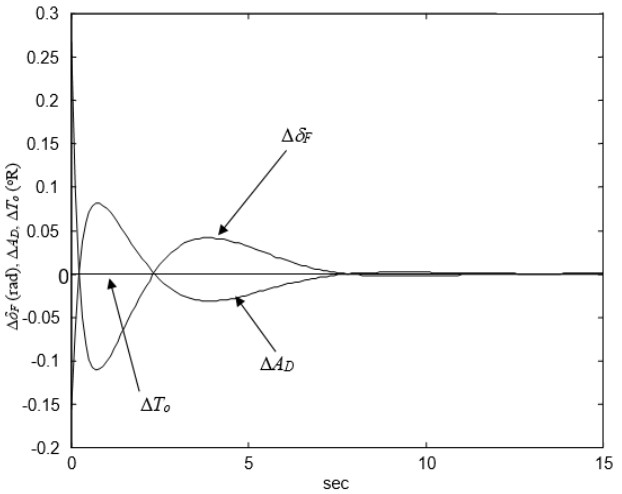

Fig. 6 $\Delta\delta_F$, ΔA_D and ΔT_o responses to an initial disturbance in height of 100ft

The structural bending oscillation with the natural frequency and damping ratio tabulated in Table II cannot be seen in any other response, however. The aircraft's height response took approximately 15 seconds to completely settle after being subjected to the initial disturbance. In Figure 6, the responses of the control inputs of the controlled aircraft are plotted against time.

These responses do not display any excessive control activity or exceed the physical limits of the controls in response to the disturbance. The change in flap angle peaked immediately at -0.12rad (-7°) and oscillated with a low frequency of approximately 1.25Hz. A similar oscillation was observed in the response of the engine diffuser area control. Both controls, however, settled after 14 seconds. It is interesting to note that there was no visible change in the temperature response across the engine combustor control. It has been shown here that using a controller design using LQR theory, the aircraft dynamic motion can be stabilised.

However, the synthesis of the optimal feedback control law presented assumes that all the state variables of $\boldsymbol{x}$ are measurable. In practical aircraft flight control systems, it is physically or economically impractical to install all the transducers which would be necessary to measure every state variable [6,7]. A *state estimator* is used, therefore, to reconstruct those aircraft state variables which are difficult or impossible to measure. The state estimator is a dynamic system whose state vector, $\boldsymbol{x_E}$, is, ultimately, a close approximation to the aircraft state vector, $\boldsymbol{x}$. The entire estimator state vector, $\boldsymbol{x_E}$, is available from the estimator for use in implementing the feedback control law. Including an estimator into the dynamics of the closed-loop system for the HST can work, but at the cost of a slight loss in optimality i.e., the resulting minimum performance index, J, for the same initial state vector $\boldsymbol{x}(0)$, is slightly higher [4,5,6].

V. USING THE LUENBERGER STATE ESTIMATOR SYSTEM WITH THE HST LONGITUDINAL MOTION WITH CONTROLLER

At this point it is intended to include the dynamics of a Luenberger optimal state estimator system into the HST dynamics. Brief details of the estimator are presented next based on [4] and [7].

For a system defined by Eqn (11) and (14), it is intended to design an estimator which will provide an estimated state vector, $\boldsymbol{x_E}$, but will require only inputs from the control vector, $\boldsymbol{u}$, and from another vector, $\boldsymbol{w}$, which is related to the output vector, $\boldsymbol{y}$. Hence,

$$\dot{\boldsymbol{x}}_{\boldsymbol{E}} = \hat{\mathrm{F}}\boldsymbol{x}_{\boldsymbol{E}} + \hat{\mathrm{G}}\boldsymbol{u} + \boldsymbol{w} \qquad (28)$$

The forcing vector $\boldsymbol{w}$ is chosen to be

$$\boldsymbol{w} = \mathrm{K_E}\left(\boldsymbol{y} - \boldsymbol{y}_{\boldsymbol{E}}\right) \qquad (29)$$

where $\mathrm{K_E}$ is the estimator gain matrix and $\boldsymbol{y_E}$ is the estimated output vector defined as:

$$\boldsymbol{y}_{\boldsymbol{E}} = \mathrm{C}\boldsymbol{x}_{\boldsymbol{E}} \qquad (30)$$

Hence,

$$\dot{\boldsymbol{x}}_{\boldsymbol{E}} = \left(\hat{\mathrm{F}} - \mathrm{K_E C}\right)\boldsymbol{x}_{\boldsymbol{E}} + \hat{\mathrm{G}}\boldsymbol{u} + \mathrm{K_E C}\boldsymbol{x} \qquad (31)$$

However, from Eqn (1),

$$\mathrm{B}\boldsymbol{u} = \dot{\boldsymbol{x}} - \mathrm{A}\boldsymbol{x} \qquad (32)$$

If $\hat{\mathrm{G}}$ = B, then

$$\dot{\boldsymbol{x}}_{\boldsymbol{E}} = \left(\hat{\mathrm{F}} - \mathrm{K_E C}\right)\boldsymbol{x}_{\boldsymbol{E}} + \dot{\boldsymbol{x}} - \left(\mathrm{A} - \mathrm{K_E C}\right)\boldsymbol{x} \qquad (33)$$

Hence,

$$\dot{x}_E - \dot{x} = \left(\hat{\mathrm{F}} - \mathrm{K_E C}\right)x_E - \left(\mathrm{A} - \mathrm{K_E C}\right)x \quad (34)$$

By choosing the coefficient matrix, $\hat{\mathrm{F}}$, of the estimator to be identical to that of the aircraft, i.e., $\hat{\mathrm{F}}$ = A, and by defining any difference between the estimated and the actual state vector to be an error vector, ***e***, it can easily be shown that:

$$\dot{\boldsymbol{e}} = \left(\mathrm{A} - \mathrm{K_E C}\right)\boldsymbol{e} \quad (35)$$

Provided that the real eigenvalues or the real parts of the eigenvalues of the matrix, $\left(\mathrm{A} - \mathrm{K_E C}\right)$ are negative, then, as $t \to \infty$, the error vector, ***e***, will tend to zero and the estimator vector, $\boldsymbol{x_E}$, will correspond to the state vector, ***x***, of the aircraft. Only $\mathrm{K_E}$ is required to obtain this condition.
Suppose

$$\dot{\boldsymbol{e}} = \hat{\mathrm{A}}\boldsymbol{e} + \hat{\mathrm{Z}}\tilde{\boldsymbol{v}} \quad (36)$$

then, to minimise $\tilde{\boldsymbol{v}}$, use the performance index:

$$J = \frac{1}{2}\int_0^\infty \left(e'Q_o e + \tilde{v}'G_o\tilde{v}\right) dt \quad (37)$$

The resultant control law is:

$$\tilde{\boldsymbol{v}}^{\boldsymbol{o}} = -\hat{\mathrm{H}}\boldsymbol{e} \quad (38)$$

where,

$$\hat{H} = G_o^{-1}\hat{Z}'\hat{P} \quad (39)$$

Substituting Eqn (38) into Eqn (36),

$$\dot{\boldsymbol{e}} = \hat{\mathrm{A}}\boldsymbol{e} + \hat{\mathrm{Z}}(-\hat{\mathrm{H}}\boldsymbol{e}) \quad (40)$$

Hence,

$$\dot{\boldsymbol{e}} = \left(\hat{\mathrm{A}} - \hat{\mathrm{Z}}.\hat{\mathrm{H}}\right)\boldsymbol{e} \quad (41)$$

If it can be arranged such that:

$$\left[\zeta.\mathrm{I} - \left(\mathrm{A} - \mathrm{K_E}.\mathrm{C}\right)\right] = \left[\zeta.\mathrm{I} - \left(\hat{\mathrm{A}} - \hat{\mathrm{Z}}.\hat{\mathrm{H}}\right)\right] \quad (42)$$

then, the optimal closed-loop estimator will be the required estimator provided that:

$$\hat{A} = A' \quad (43)$$

$$\hat{Z} = C' \quad (44)$$

and

$$\hat{H} = K_E{}' \quad (45)$$

Using LQR theory, the optimal feedback gain matrix for the closed-loop estimator can be conveniently found. The aircraft dynamics with the estimator system included can be represented by the block diagram of Figure 7.

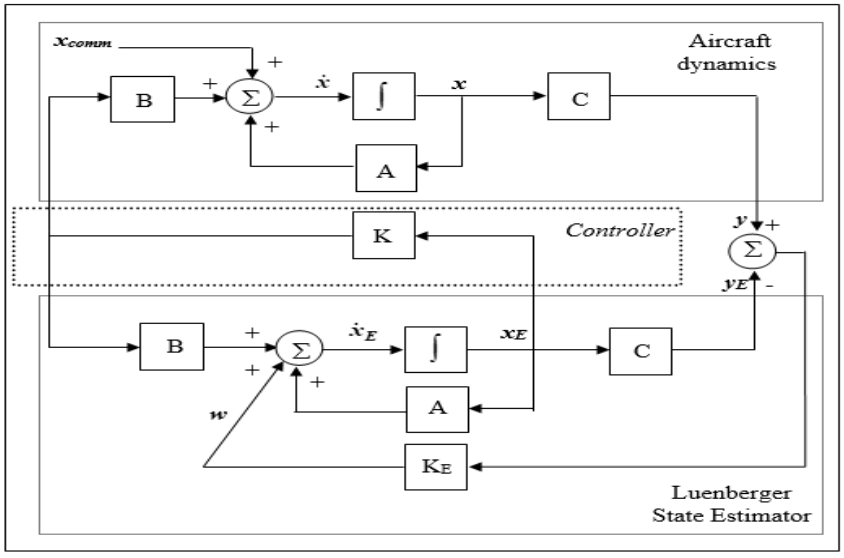

Fig. 7 The aircraft dynamics with an estimator system included. $\mathrm{K_E}$ is the Luenberger estimator gain matrix

It should be noted that the ability to reconstruct the aircraft state variables from the output of the aircraft dynamics requires that the state variables be observable. The necessary condition for complete observability is given by Eqn (46).

$$\mathrm{Rank}\begin{bmatrix} \mathrm{C} \\ \mathrm{CA} \\ \mathrm{CA}^2 \\ \vdots \\ \mathrm{CA}^{n-1} \end{bmatrix} = \mathrm{n} \quad (46)$$

n is the dimension of the aircraft state vector.

It should be noted that when calculating the Luenberger estimator gain matrix, $\mathrm{K_E}$, using Matlab Control System Toolbox, the algorithm used is the same as when calculating the optimal feedback gain matrix for the aircraft closed-loop system. But instead of using the matrix, A, as the plant matrix, A^T is used (See Eqn (43)) and likewise, instead of using the matrix, B, as the driving matrix, C^T (See Eqn (44)), is used.

The theoretical requirements that the matrix, $\mathrm{Q_o}$, has to be at least positive semidefinite and the matrix, $\mathrm{G_o}$, must be positive definite in Eqn (37) must also be observed.

Here, it is assumed that the only measurable state variables which can be obtained from the HST are $\Delta\alpha$, Δq and Δh. Hence, for the aircraft dynamics output equation, Eqn (14), the matrix C, is:

$$C = \begin{bmatrix} 0 & 1 & 0 & 0 & 0 & 0 & 0 \\ 0 & 0 & 1 & 0 & 0 & 0 & 0 \\ 0 & 0 & 0 & 0 & 1 & 0 & 0 \end{bmatrix} \qquad (47)$$

To ensure that the estimator can estimate all the state variables of the aircraft, the dynamics of the aircraft have to be observable. Using Eqn (46), the rank of the corresponding observability matrix was 7, the same as the dimension, n, of the state vector. Hence, the aircraft dynamics are observable, and an estimator can be designed.

To obtain the gain matrix of the Luenberger estimator, the performance index Eqn (37) was minimised. Any persistent difference between the state vector of the estimator and the state vector of the aircraft was penalised by use of the state weighting matrix, Q_o, viz.,

$$Q_o = \text{diag}\begin{bmatrix} 0.1 & 0.01 & 0 & 0.1 & 1 & 0 & 0 \end{bmatrix} \qquad (48)$$

The choice of elements of matrix, Q_o, was arbitrary, but its positive semidefinite nature was maintained. Since there are three measurable state variables, the matrix, G_o, is of order (3×3). Again, the choice of the diagonal elements of this matrix was also arbitrary but the matrix was required by theory to be positive definite, viz.,

$$G_o = \begin{bmatrix} 1 & 0 & 0 \\ 0 & 1 & 0 \\ 0 & 0 & 1 \end{bmatrix} \qquad (49)$$

The solution, $\hat{P}$, to the algebraic Riccati equation resulted in the minimisation of the performance index. Then, using Eqn (39), the Luenberger estimator gain matrix was obtained, viz.

$$K_E' = \begin{bmatrix} -18.4 & -44.1 & -3.7 \\ 0.7 & 1.7 & 0.1 \\ 1.7 & 4.0 & 0.3 \\ 0.7 & 1.7 & 0.4 \\ 0.1 & 0.3 & 72.2 \\ 0.1 & 0.3 & 0.02 \\ 0.3 & 0.8 & 0.01 \end{bmatrix} \qquad (50)$$

The responses of the aircraft with the estimator operating are presented next. Figure 8 shows the height response of the aircraft with the Luenberger estimator subjected to an arbitrary commanded step input. The response shows that the controlled aircraft, using in the feedback control the state vector reconstructed in the Luenberger estimator, was stable.

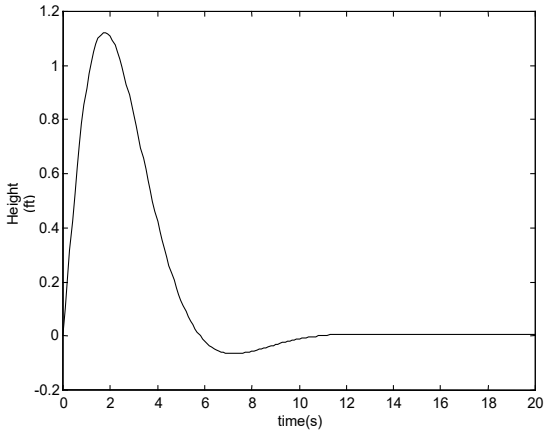

Fig. 8 The change in height response (Δh) of Hyperion with a Luenberger estimator

The height response of the estimator was virtually identical to that shown by the aircraft height output. This is easily confirmed by plotting the difference between both responses against time, as presented in Fig. 9.

The maximum difference occurred instantaneously as a result of the step-input command, but this difference did not persist. No difference was visible between the aircraft output, $\boldsymbol{y}$, and the estimator output, $\boldsymbol{y_E}$, after 0.2 second. Similar results were obtained for other output variables.

It has been shown here that a suitable controller designed using LQR theory and a Luenberger state estimator can be incorporated into the HST dynamics.

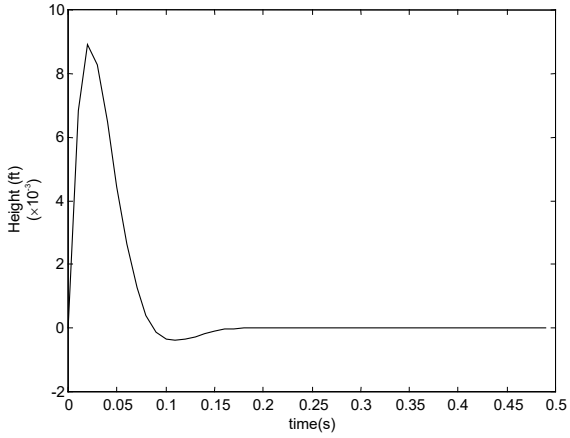

Fig. 9 The difference between the aircraft height output and the estimator height output

VI. LUENBERGER ESTIMATOR ABILITY TO REDUCE SENSOR AND PROCESS NOISES

So far, in this presentation of the research work conducted on the HST, any effect of noise or disturbances on the aircraft closed-loop stability has been neglected. In this section, the effects of sensor and process noise on the aircraft closed-loop dynamics are examined. The situation can be represented symbolically using the block diagram of Fig. 10.

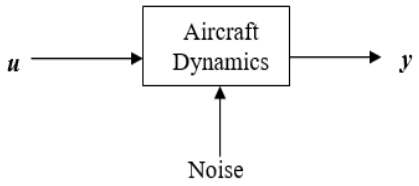

Fig. 10 Measurable output vector, ***y***

To reduce the level of noise, the signals from the aircraft output have to be filtered. A study by Chen and Chung [12] used Luenberger estimator as noise estimator but not as a noise filter. In this section, the Luenberger estimator is shown to have a capability to reduce noises without a prior knowledge of the noise characteristics.

When designing an AFCS for an aircraft, the only signal available to indicate any changes in the aircraft dynamics is the output signal, ***y***, which is measured using sensors on the aircraft which detect changes in, for example, atmospheric pressure, attitude changes or structural bending. When a change in the aircraft state is required, a control input signal, ***u***, is supplied by the pilot or the AFCS to cause the aircraft controls to change/deflect appropriately. The sensors then detect any changes in the aircraft state, caused by these changes in the control inputs. The output signal, ***y***, is usually not a smooth signal, however. The signal is often contaminated with noise from the sensors themselves and also from other sources such as atmospheric turbulence. But at heights where the HST is to fly during the scramjet engine phase i.e., at heights between 80000ft and 100000ft, atmospheric turbulence is minimal [13].

To account for how such noise could affect the closed-loop dynamics of the HST, consider the two types of noises commonly associated in AFCS studies. The first type, process noise, appears in the form of atmospheric turbulence; and the second is sensor noise i.e., the noise inherent in any sensor measuring an aircraft output signal. The effect of these noise sources resulted in considerable difficulty in identifying the original 'clean' output signal of the aircraft in the response to the same stimulus in the absence of noise.

Fig. 11 shows the mathematical model of the controlled aircraft using a state estimator. The points at which the process and sensor noise, ***w*** and ***v*** respectively, were inserted into the aircraft dynamics are clearly shown.

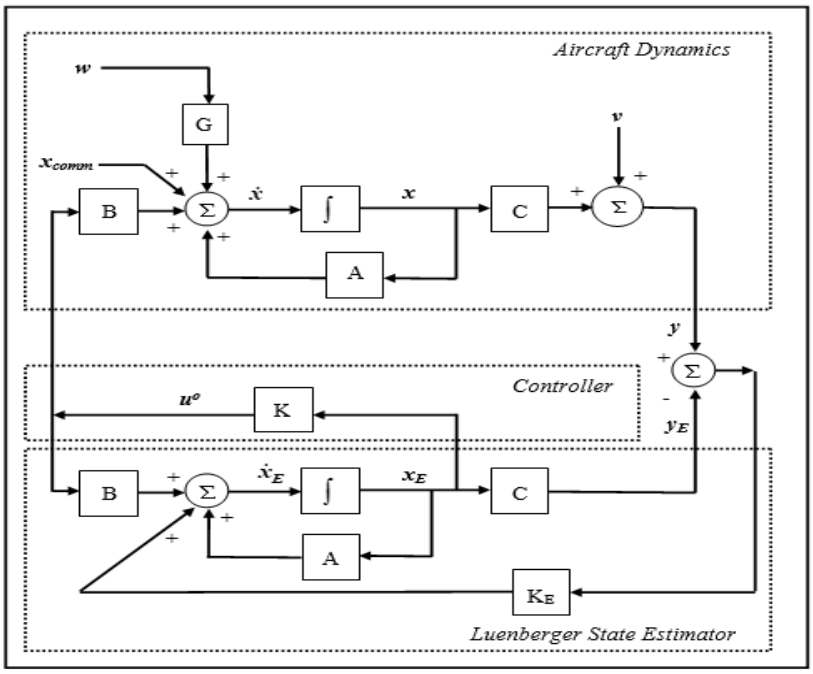

Fig. 11 Block diagram of an aircraft mathematical model with an estimator system but also with noise inputs

The estimator gain matrix is denoted by K_E. The optimal feedback gain matrix of the controller is K. The output of this aircraft is ***y*** and that of the estimator is $\boldsymbol{y_E}$. The properties of the noise inputs are presented next. First, note that the block diagram in Fig.11 assumes additive noise only. It was also assumed that the noise was injected at two points only. This meant that any noise entering with the optimal control, $\boldsymbol{u^o}$, is equivalent to some other noise entering at the same point as ***w***. Noise from the sensors that contaminate the aircraft output signal, ***y***, is equivalent to adding a noise term, ***v***, to the output signal.

Both noises, ***w*** and ***v***, were assumed to be white, Gaussian, and to have zero mean. The first property implies that the noises were uncorrelated from instant to instant. The second property implies that all probabilistic information about the noise were summed up in the covariance of the noise e.g., E [$\boldsymbol{v.v'}$] for ***v***. E(X) is the expectation of X which is also known as the mean or average value of X over an infinite number of X. It will be shown here that the Luenberger estimator which will also double as a noise filter, is capable of significantly reducing the level of noise in the HST dynamics without any a priori knowledge of the noise characteristics.

The performance of the noise filter will be measured by calculating the covariance of the vector $\hat{\boldsymbol{e}}$ where $\hat{\boldsymbol{e}} = \boldsymbol{y} - \boldsymbol{y}_E$ i.e., the difference between the aircraft output, $\boldsymbol{y}$, and the estimated output, $\boldsymbol{y}_E$. $\hat{\boldsymbol{e}}$ can also be taken as the noise rejected by the filter from the aircraft output signal. The size of the covariance of $\hat{\boldsymbol{e}}$ indicates the amount of noise that has been filtered out. Because the noises added into the aircraft dynamics are characterised in terms of their covariance, comparison of the covariance of noise rejected by the filter, $\hat{\boldsymbol{e}}$, can easily be made. The activities of the control inputs of the aircraft were also plotted against time and the rms values were calculated to determine the existence of any excessive control responses.

Chalk [11] has concluded that the probability of encountering turbulence decreases from 80% at sea level to only 7% at an altitude of 40000ft. Similar conclusions were made by Ehemberger [12]. In this paper, the process noise, $\boldsymbol{w}$, was assumed to be small (zero mean with variance of 1×10^{-5} ft^2) therefore, because at 85000ft the air density is low and hence, the effect of air turbulence may be assumed to be negligible.

The sensor measuring the change in height of the aircraft had added noise, $\boldsymbol{v}$, which was assumed to have Gaussian distribution, zero mean and an arbitrary standard deviation (σ_s) of 0.03ft [10]. Hence, the variance of the sensor noise (σ_s^2) is 0.0009 ft^2. No cross correlation between $\boldsymbol{w}$ and $\boldsymbol{v}$ was assumed.

The estimator gain matrix, Eqn (50) of the Luenberger estimator was used again here to test its noise rejection capability. The HST with its AFCS was subjected to the same initial disturbance as before, i.e., 100ft in height. The response of the aircraft with the Luenberger estimator is shown below.

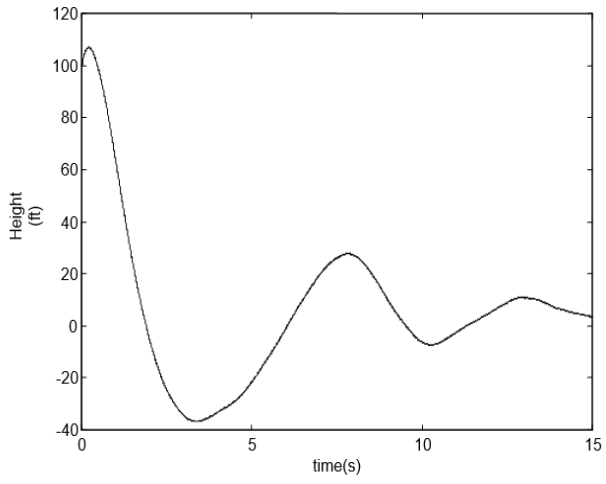

Fig. 12 The response in height from the aircraft output, $\boldsymbol{y}$, with a Luenberger estimator when subjected to an initial disturbance in height of 100ft

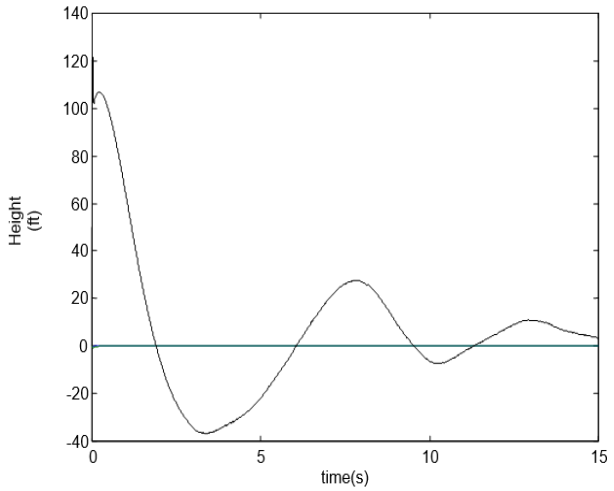

Fig. 13 This is the response from the same aircraft but from the Luenberger estimator output, $\boldsymbol{y}_E$

From inspection, the estimator appears to have reduced the noise level in the system. The variance of $\boldsymbol{y}$ was found to be 4.995ft^2 but the variance of $\boldsymbol{y}_E$ was 4.9943. The variance of noise rejected by this estimator was calculated to be 0.001ft^2. Note that the variance of the sensor noise was 0.0009ft^2 and that the variance of noise rejected by the estimator is close to this value. Fig. 14 shows a close-up view of the responses measured from the aircraft dynamics and that from the estimator together.

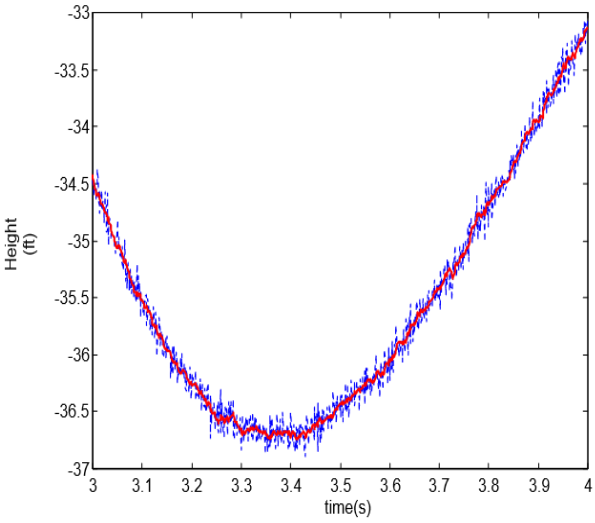

Fig. 14 The responses, $\boldsymbol{y}$ (dotted) and $\boldsymbol{y}_E$ (bolded) between 3s and 4s

It has been shown here that the Luenberger estimator can be used effectively to filter noise in the AFCS for the HST.

The response of the flaps control is shown in Fig. 15. When the disturbance was initiated, the response of the flaps appeared to deflect upwards to 30 rad and then rapidly deflected downwards to –5 rad. Then, the response appeared to settle with little noise effect from the sensor appeared on the response.

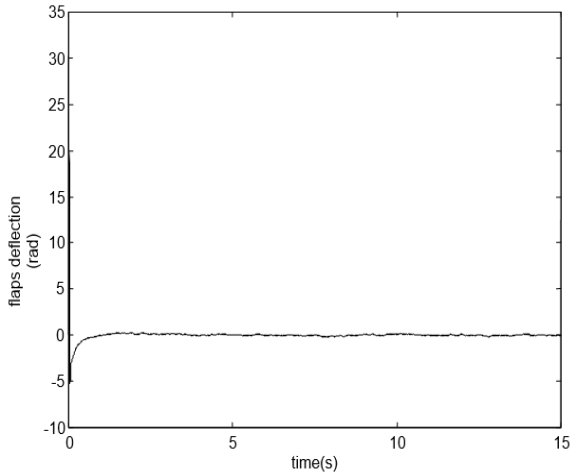

Fig. 15 Flaps response of the aircraft with the Luenberger estimator when sensor noise contaminates the aircraft output signal

The large deflection in the initial part of the simulation when the HST was subjected to the initial disturbance can be a cause for concern because the angle of deflection could never physically be achieved by any flaps actuator system. Moreover, large angles of deflection will cause excessive aerodynamic heating to the flaps during hypersonic flight. Also, in this simulation, no limiter was used to limit the deflection of the flaps. A realistic limit to flap deflection during hypersonic flight is beyond the scope of this paper. However, it will be shown here that the flaps maximum angle of deflection can be limited whilst maintaining the aircraft dynamic stability. In the next simulation, the flaps have been arbitrarily limited to deflect between +45 degree (+0.7850rad) and -45degree (-0.7850rad). The simulation shows that the stability of the HST is still maintained even though the angle of deflection of the flaps has been restricted.

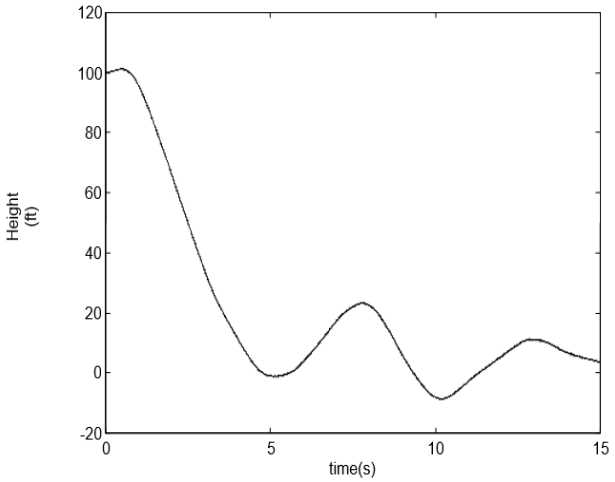

Fig. 16 Aircraft height output, $\boldsymbol{y}$, for aircraft with restricted flaps deflection

The aircraft with the Luenberger estimator and the sensor noise problem was subjected to the same initial disturbance in height again and the response of the aircraft height change can be seen in Fig. 16. The response shows that even with the flap's limiter used, the aircraft stability is maintained.

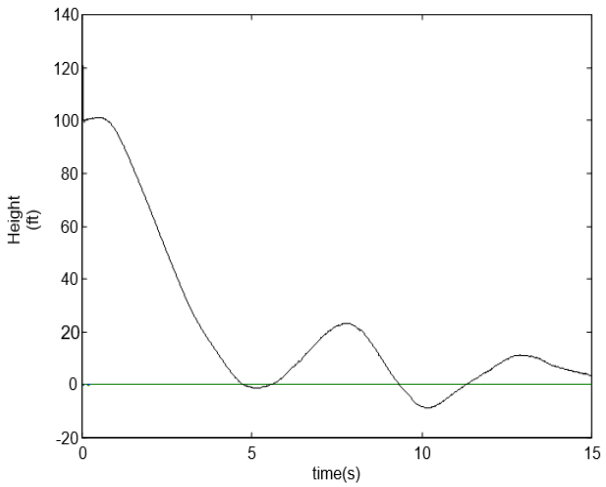

Fig. 17 Estimator height output, $\boldsymbol{y_E}$, for aircraft with restricted flaps deflection

The response of the estimator in Fig. 17 appeared to be the same as that measured from the aircraft output shown in Fig. 16. To investigate visually if the noise has been reduced by this Luenberger estimator, responses from the aircraft output, $\boldsymbol{y}$, and from the estimator output, $\boldsymbol{y_E}$, were plotted together on the same axis. This can be seen in Fig. 18.

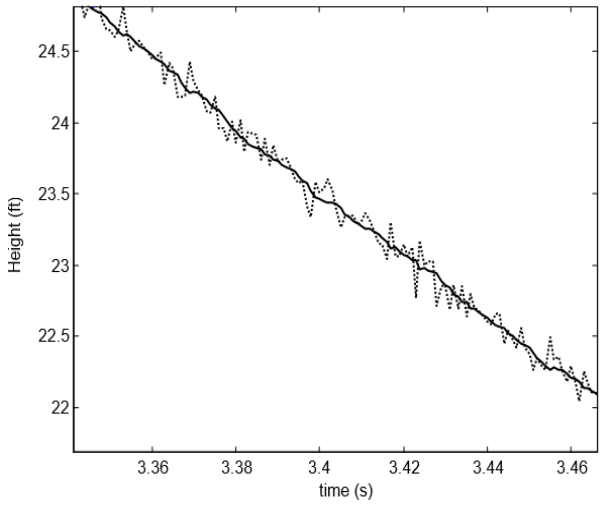

Fig. 18 The responses, $\boldsymbol{y}$ (dotted) and $\boldsymbol{y_E}$ (bolded) between 3.34s and 3.47s

From Fig. 18, noise reduction has occurred. The response of the flaps was investigated again. Because a limiter has been used to prevent excessive deflection, the flaps first deflected upwards to 0.7850 rad and then immediately deflected downwards to -0.7850 rad.

However, the flaps fluctuate between approximately +0.2 rad (11.5°) and -0.2 rad (-11.5°) after the 1st second of simulation. The response had a rms value of 0.39rad. These values are less than those obtained when using the first Luenberger estimator.

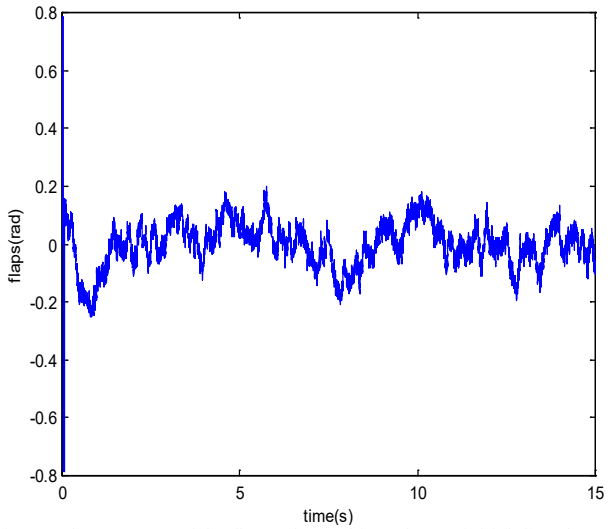

Fig. 19 The response of the flaps when subjected to an initial disturbance

The results of these tests show that the Luenberger estimator can be an effective aircraft state estimator as well as noise filter. The obvious advantage of using the Luenberger estimator, as a noise filter for HST flying at a range of high Mach numbers and heights, is that no prior knowledge of the noise is required. When data on atmospheric disturbances at those speeds and heights flown by HST are scarce, this technique has an added advantage.

VII. CONCLUSION

This paper has described how the highly unstable longitudinal motion of Hyperion can be stabilised by a S.A.S designed using LQR theory. This theory has considerable practical advantages for use in AFCS design since it guarantees closed-loop dynamic stability. The optimal control law requires that all the state variables of the aircraft be measurable. Since this is impractical, a Luenberger estimator was designed and included in the HST. The dynamics of the aircraft with the controller and the estimator operating were found to remain stable. It was found also that the response of the estimated state vector quickly reached that of the aircraft when the aircraft was subjected to initial disturbances or to command inputs. This experiment also examined the effect of noise on the aircraft dynamics. The aircraft output, $\boldsymbol{y}$, was measured using some sensors but using these sensors introduced noise into the measured signals. Another source of noise might be atmospheric turbulence. The effect of sensor noise on the aircraft output signal, $\boldsymbol{y}$, was significant. The tests showed that using a Luenberger estimator can result in a significant amount of noise reduction in the aircraft output signal. In designing a Luenberger estimator the characteristics of the process and sensor noises need not be considered a priori when calculating the estimator gain matrix. This is an advantage for HST work as the noise characteristics when the aircraft flies at high Mach numbers and altitudes are not entirely certain.

REFERENCES

[1] Y. Ding, X. Wang and Y. Bai, *et al.,* "An improved continuous sliding mode controller for flexible air-breathing hypersonic vehicle," *Int.J. Robust Nonlinear Control*, Vol. 30, No. 14, pp. 5751-5772, 2020.

[2] S. Liang, B. Xu and J. Ren, "Kalman-filter-based robust control for hypersonic flight vehicle with measurement noises," *Aerospace Science and Technology*, Vol. 112, DOI: https://doi.org/10.1016/J.AST.2021.106566

[3] J. Sun, J. Yi and Z. Pu, "Augmented fixed-time observer-based continuous robust control for hypersonic vehicles with measurement noises," *IET Control Theory Appl*., Vol. 13, No. 3, pp. 422-433, 2019.

[4] B. D. O. Anderson and J. B. Moore, *Linear Optimal Control,* New Jersey: Prentice-Hall Inc., 1971.

[5] M. Athans and P. L. Falb, *Optimal Control - An Introduction to the Theory and Its Applications,* New York: McGraw-Hill, 1966.

[6] A. E. Bryson and Y.C. Ho, *Applied Optimal Control,* New York: Hemisphere, 1975.

[7] D. McLean, *Automatic Flight Control System*, Hemel Hempstead: Prentice Hall, 1993.

[8] L. J. Ehemberger, "Stratosphere Turbulence Measurements and Models for Aerospace Plane Design," NASA, *NASA Technical Memorandum,* 104262, 1992.

[9] F. R. Chavez and D. K. Schmidt, "Analytical Aeropropulsive/ Aeroelastic Hypersonic-Vehicle Model with Dynamic Analysis*, "Journal of Guidance, Control and Dynamics*, Vol. 17, No. 6, pp. 1308-1319, 1994.

[10] Z. A. Zaludin, "Mathematical Model of An Aircraft Flying Over a Range of Hypersonic Speeds and Heights," *Aeronautics and Astronautics Department, Southampton University, Southampton, Technical Report: AASU 98/01,* 1998.

[11] C. R. Chalk, T. P. Neal, T. M. Harris, F. E. Pritchard, and R. J. Woodcock, "Background Information and User Guide for Military Specification of Flying Qualities of Aircraft," *Air Force Flight Dynamics Lab. Tech. Report*, pp. 69-72, 1969.

[12] G. Chen, and S. H. Chung, "Depth Control of a submersible vehicle under a seaway using a noise estimator," *Proceedings for Sixth International Conference on Electronic Engineering in Oceanography*, Cambridge, UK, pp. 30-34, 1994.

[13] W. S. Widnall, and P. K. Sinha, "Optimizing the Gains of the Baro-Inertial Vertical Channel," *Journal of Guidance, Control and Guidance*, Vol. 3, No. 2, pp. 172-178, 1980.